Journal of Materials Chemistry C

Efficient white polymer light-emitting diodes (WPLEDs) based on double emitting layers of PVK:Eu(III)-complex and Alq3

Journal:	*Journal of Materials Chemistry C*
Manuscript ID	TC-ART-12-2018-006610.R1
Article Type:	Paper
Date Submitted by the Author:	21-Feb-2019
Complete List of Authors:	Hui, Yani; Northwest University Liu, Lin; Northwest Univeristy, Fu, Guorui; Northwest University, Li, Wentao; Northwest University Lv, Xingqiang; Northwest University, ; Hong Kong Baptist University, Department of Chemistry He, Hongshan; Eastern Illinois University, Chemistry Wong, Wai-Yeung; The Hong Kong Polytechnic University, Faculty of Applied Science and Textiles

Journal Name

ARTICLE

Efficient white polymer light-emitting diodes (WPLEDs) based on double emitting layers of PVK:Eu(III)-complex and Alq_3

Received 00th January 20xx,
Accepted 00th January 20xx

DOI: 10.1039/x0xx00000x

www.rsc.org/

Yani He,[a‡] Lin Liu,[a,b‡] Guorui Fu,[a] Wentao Li,[a] Xingqiang Lü[a,*], Hongshan He[c,*] and Wai-Yeung Wong[d,*]

Colour-tunable polymer light-emitting diodes (PLEDs) were realized by tuning the concentration of a Eu^{3+}-complex in the emitting-layer (EML) and the thickness of the hole-blocking BCP layer (BCP = 2,9-dimethyl-4,7-diphenyl-1,10-phenanthroline) in a double-emitting-layer (dEML) configuration. The dEML used PVK:complex **2** (PVK = poly(*N*-vinylcarbazole); H_2Salen = *N*,*N*'-bis(salicylidene)cyclohexane-1,2-diamine and HDBM = dibenzoylmethane for [Zn(Salen)(μ-OAc)Eu(DBM)$_2$)] (**2**)) as the EML1 and Alq_3 as the EML2. The efficiencies (0.32-0.39 cd A^{-1}, 0.54-0.56% and 0.99-1.10 lm W^{-1}) were obtained from organo-Eu^{3+} incorporated WPLEDs with the complex-**2**-doping content of 20 or 30 wt% and 20 nm of the BCP thickness. The WPLEDs exhibited low turn-on voltage (6.0-7.5 V) and low efficiency-roll-off, which are advantageous to organo-Eu^{3+} doped WOLEDs.

1. Introduction

White-light from the facile integration of *di*-, *tri*- or *tetra*-chromatic colour[1] with primary red-light from Eu^{3+} ion is highly attractive owing to its potential applications[2] in full-colour flat-panel display and solid-state lighting. For example, commercially-available white light-emitting diodes (WLEDs) used inorgano-Eu^{3+} as the red-light source and the technology is pretty mature.[3] However, several shortcomings especially the formation of clusters, are difficult to overcome. By contrast, organo-Eu^{3+} based counterparts[4] offer several distinctive advantages including broadened photo- and electro-luminescent spectra and versatile structural modifications. Extensive researches of organo-Eu^{3+} incorporation using small-molecule Eu^{3+}-complex,[5] Eu^{3+}-based coordination polymer[6] and doping of Eu^{3+}-complex[7] or grafting system[8] are focused on inorganic-chip-hybridized UV or near-UV (NUV) WLEDs, while the realization of typically reliable and efficient white organic light-emitting diodes (WOLEDs)[9] based on organo-Eu^{3+} phosphor is much less explored.

Several approaches for organo-Eu^{3+} incorporated WOLEDs have been reported. The milestone work[10] by using an organo-Eu^{3+} active emitting-layer (EML) by Kido et al. has been devoted to organo-Eu^{3+} complexes with specific structures for WOLEDs as potential high-performance alternatives to the existing low-efficiency incandescent and fluorescent lights. The approach relied on volatile organo-Eu^{3+} complexes capable of fabricating single-molecule[11] or single-component white-light.[12] The WOLEDs from this approach showed low η_{EQE} (< 0.1%) due to incomplete energy transfer for organo-Eu^{3+} single-molecule white-light.[11] Some WOLEDs showed relatively higher efficiency (η_{EQE}^{max} up to 1.1%), however, notorious crystallization and thermal-dissociation induced efficiency-roll-off (up to 50%) was observed.[12] In addition, inevitable high-cost from vacuum-deposition procedure impedes its popularity. To circumvent such problems, it is desirable to dope organo-Eu^{3+} guest into a small-molecule or polymer host for a solution-processed WOLED[13] or WPLED[14] (white polymer light-emitting diode). Colour-tuning white-light could be smoothly modulated within the host-guest-constituted mono-emitting-layer (mEML), however, it is difficult to choose proper host materials to ensure the low-lying highest occupied molecular orbital (HOMO) and lowest unoccupied molecular orbital (LUMO) aligned properly.[15] Effective carrier injection and balance for satisfactory electro-luminescent efficiencies are also much difficult to be guaranteed.[13-14] Moreover, the long phosphorescent lifetimes of the excited state of organo-Eu^{3+} complexes often undergo the excitons' saturation[16] particularly at high current density. Severe triplet-triplet annihilation resulted from localized excitons' aggregation and doping-induced phase separation give rise to a detrimental inconsistent performance (colour and efficiency).[13-14] Inspired by a conceptual strategy to double-EML (dEML) device architecture,[17] which was known to be effective in both improving efficiency and delaying efficiency-roll-off for transition-metal-complex based OLEDs,[18] we used a Eu^{3+}-complex as high colour-purity red-light source coupled with Alq_3 to address these problems. On one hand, holes in the EML1 and electrons in the EML2 are provided to broaden the recombination zone, from which confinement of charge carriers at the interface of hole- and electron-dominant EMLs with stepwise energy levels, significant performance improvement should be considerably favoured.

[a]*School of Chemical Engineering, Shaanxi Key Laboratory of Degradable Medical Material, Northwest University, Xi'an 710069, Shaanxi, China.*
[b]*School of Chemistry and Chemical Engineering, Yanan University, Yanan 716000, Shaanxi, China*
[c]*School of Chemistry, Eastern Illinois University, Charleston, IL 61920, USA*
[d]*Department of Applied Biology and Chemical Technology, The Hong Kong Polytechnic University, Hung Hom, Hong Kong, P.R. China*
**E-mail: lvxq@nwu.edu.cn; hhe@eiu.edu; wai-yeung.wong@polyu.edu.hk; Tex/Fax: +86-29-88302312*
Electronic Supplementary Information (ESI) available: [Starting materials and characterization; XRD; UV, PL]. See DOI: 10.1039/x0xx00000x
‡ These authors contributed equally and should be considered *co*-first authors.

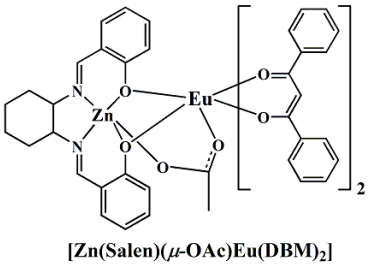

[Zn(Salen)(μ-OAc)Eu(DBM)$_2$]

Scheme 1. Structure scheme of complex [Zn(Salen)(μ-OAc)Eu(DBM)$_2$)] (**2**).

Herein, we reported the synthesis of a [Zn(Salen)]-based Eu^{3+}-complex, [Zn(Salen)(μ-OAc)Eu(DBM)$_2$)] (**2**) shown in Scheme 1, and its application of dEML-characteristic devices. The WPLEDs with PVK:complex **2** as the EML1 and Alq_3 as the EML2 of Alq_3 were fabricated. The blue-light[19] (λ_{em} = 420 nm) from PVK, red-light (λ_{em} = 613 nm) from complex **2** and green-light[20] (λ_{em} = 512 nm) from Alq_3 enabled the typical *tri*-chromatic white-light production. Upon the distribution of complex **2** into the PVK host, effective Förster energy transfer[21] from PVK to complex **2** can be activated. The high hole mobility[19] of the PVK host renders the EML1 characteristic of hole-domination. The modest triplet energy[20] of the separated EML2 (Alq_3) between PVK and complex **2**, suppresses energy back transfer from complex **2** to Alq_3.[22] More importantly, the electron-transporting[20] Alq_3 (EML2) could act as energy transfer ladder.[17-18] As a result, carriers can be confined within that dEML zone. Further thorough optimization of the doping concentration of complex **2** in the EML1 and the thickness of BCP to elaborate the hole-blocking for desirable carriers' balance, high-efficiency with low efficiency-roll-off are specifically pursued.

2. Experimental section

The information for starting materials and general characterization methods has been described in the Electronic Supporting Information (ESI). The Schiff-base ligand H_2Salen was rationally synthesized from the condensation reaction between an equimolar mixture of *cis*- and *trans*-1,2-diaminocyclohexane and salicylaldehyde according to the literature.[23]

Synthesis of precursor [Zn(Salen)(MeCN)]

To a stirred solution of the ligand H_2Salen (0.645 g, 2 mmol) in dry MeCN (20 mL), an equivalent amount (0.440 g, 2 mmol) of solid $Zn(OAc)_2{\cdot}2H_2O$ was added, and the resulting mixture was heated under reflux for 3 h. After cooling to room temperature, the insoluble yellow precipitate was filtered, washed with absolute CH_2Cl_2 (5 mL) three times, and dried at 45 °C under vacuum to a constant weight. Yield: Yield: 0.776 g (91%). Anal. Calcd for $C_{22}H_{23}N_3O_2Zn$: C, 61.91; H, 5.43; N, 9.84%. Found: C, 61.83; H, 5.52; N, 9.79%. FT-IR (KBr, cm^{-1}): 3051 (w), 2933 (w), 2858 (w), 2360 (w), 1629 (s), 1600 (w), 1571 (m), 1537 (m), 1465 (w), 1444 (s), 1396 (w), 1338 (w),1307 (m), 1186 (m), 1145 (w), 1122 (w), 1020 (w), 983 (w), 906 (m), 854 (w), 792 (w), 756 (vs), 673 (m), 601 (w), 559 (w), 530 (w), 505 (w), 455 (w), 408 (w). ^{1}H NMR (400 MHz, DMSO-d_6): δ (ppm) 8.31 (s, 2H, -CH=N), 7.19 (t, 2H, -Ph), 7.11 (t, 2H, -Ph), 6.60 (m, 2H, -Ph), 6.40 (t, 2H, -Ph), 3.17 (s, 2H, -Cy), 2.44 (m, 2H, -Cy), 2.08 (s, 3H, -CH_3), 1.89 (m, 2H, -Cy), 1.37 (m, 4H, -Cy). ESI-MS (MeCN) *m/z*: 426.12 (100%, $[M-H]^+$).

Synthesis of complexes [Zn(Salen)(μ-OAc)Ln(DBM)$_2$)] (Ln = La, 1; Ln = Eu, 2, Ln = Tb, 3 or Ln = Gd, 4)

To a dry $CHCl_3$ solution (10 mL) of the typical β-diketonate ligand HDBM (dibenzoylmethane; 0.8 mmol, 0.180 g) deprotonated by an equimolar amount of solid KOH (0.8 mmol, 0.044 g), another MeOH solution (4 mL) of $Ln(OAc)_3{\cdot}6H_2O$ (0.4 mmol; Ln = La, 0.170 g; Ln = Eu, 0.174 g; Ln = Tb, 0.172 g; Ln = Gd, 0.176 g) was added, and the resultant mixture was refluxed for 3 h. After cooling to room temperature, the complex precursor [Zn(Salen)(MeCN)] (0.4 mmol, 0.170 g) was added, and the resulting mixture was refluxed for another 3 h. Each of the clear yellow solutions was cooled to room temperature and filtered. Diethyl ether was diffused into the respective filtrate at room temperature and pale yellow microcrystalline solids of complexes **1**-**4** were obtained in about three weeks, respectively.

[Zn(Salen)(μ-OAc)La(DBM)$_2$)] (**1**): Yield: 0.326 g (79%). Anal. Calcd for $C_{52}H_{45}N_2O_8ZnLa$: C, 60.62; H, 4.40; N, 2.72%. Found: C, 60.60; H, 4.42; N, 2.74%. FT-IR (KBr, cm^{-1}): 3059 (w), 2935 (w), 1637 (w), 1598 (m), 1550 (s), 1519 (vs), 1478 (s), 1456 (m), 1399 (s), 1305 (w), 1223 (w), 1193 (w), 1155 (w), 1125 (w), 1071 (w), 1024 (w), 941 (w), 905 (w), 847 (w), 785 (m), 753 (w), 722 (m), 689 (w). ^{1}H NMR (400 MHz, DMSO-d_6): δ (ppm) 8.42 (s, 1H, -C=N), 8.32 (s, 1H, -C=N), 8.02 (d, 8H, -Ph), 7.40 (m, 12H, -Ph), 7.20 (t, 2H, -Ph), 7.12 (m, 2H, -Ph), 6.73 (m, 2H, -CH=), 6.62 (m, 2H, -Ph), 6.41 (t, 2H, -Ph), 3.72 (s, 1H, -Cy), 3.20 (s, 1H, -Cy), 2.46 (d, 1H, -Cy), 2.04 (d, 1H, -Cy), 1.90 (d, 1H, -Cy), 1.74 (s, 3H, -OAc), 1.56 (d, 1H, -Cy), 1.42 (m, 4H, -Cy). ESI-MS (MeCN) *m/z*: 1029.16 (100%, $[M-H]^+$); 969.14 (23%, $[M-OAc]^+$).

[Zn(Salen)(μ-OAc)Eu(DBM)$_2$)] (**2**): Yield: 0.338 g (81%). Anal. Calcd for $C_{52}H_{45}N_2O_8ZnEu$: C, 59.86; H, 4.34; N, 2.68%. Found: C, 59.84; H, 4.37; N, 2.63%. FT-IR (KBr, cm^{-1}): 3058 (w), 2932 (w), 1638 (w), 1598 (m), 1549 (s), 1518 (vs), 1478 (s), 1455 (m), 1397 (s), 1303 (w), 1221 (w), 1193 (w), 1155 (w), 1125 (w), 1071 (w), 1024 (w), 941 (w), 906 (w), 847 (w), 785 (m), 754 (m), 722 (m), 689 (w). ESI-MS (MeCN) *m/z*: 1043.18 (100%, $[M-H]^+$); 983.15 (27%, $[M-OAc]^+$).

[Zn(Salen)(μ-OAc)Tb(DBM)$_2$)] (**3**): Yield: 0.344 g (82%). Anal. Calcd for $C_{52}H_{45}N_2O_8ZnTb$: C, 59.47; H, 4.32; N, 2.66%. Found: C, 59.45; H, 4.35; N, 2.68%. FT-IR (KBr, cm^{-1}): 3059 (w), 2932 (w), 1640 (m), 1598 (m), 1549 (s), 1517 (vs), 1478 (s), 1455 (m), 1398 (s), 1303 (m), 1221 (w), 1193 (w), 1156 (w), 1125 (w), 1070 (w), 1024 (w), 941 (w), 905 (w), 849 (w), 785 (m), 753 (m), 721 (m), 691 (w). ESI-MS (MeCN) *m/z*: 1049.18 (100%, $[M-H]^+$); 989.16 (19%, $[M-OAc]^+$).

[Zn(Salen)(μ-OAc)Gd(DBM)$_2$)] (**4**): Yield: 0.336 g (80%). Anal. Calcd for $C_{52}H_{45}N_2O_8ZnGd$: C, 59.56; H, 4.32; N, 2.67%. Found: C, 59.54; H, 4.35; N, 2.70%. FT-IR (KBr, cm^{-1}): 3059 (w), 2932 (w), 1639 (w), 1598 (m), 1549 (s), 1518 (vs), 1478 (s), 1455 (m), 1398 (s), 1303 (w), 1221 (w), 1193 (w), 1155 (w), 1125 (w), 1071 (w), 1025 (w), 941 (w), 906 (w), 851 (w), 785 (m), 754 (m), 721 (m), 689 (w). ESI-MS (MeCN) *m/z*: 1050.18 (100%, $[M-H]^+$); 988.16 (24%, $[M-OAc]^+$).

Fabrication of PLEDs-I-II based on EML1 of PVK:complex 2 and EML2 of Alq_3

Details of the fabrication and testing of the **PLEDs-I-II** are presented in the ESI. In these materials, ITO (Indium tin oxide)-coated glass was used as a substrate, and PEDOT:PSS (poly(3,4-ethylenedioxythiophene):poly(styrenesulfonate)) was used as the hole injection material. BCP (2,9-dimethyl-4,7-diphenyl-1,10-phenanthroline) was used to block hole-transport. With the doping

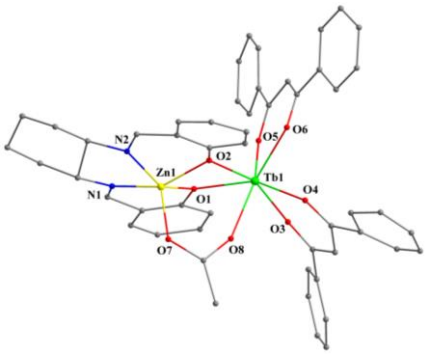

Figure 1. Perspective drawing of the hetero-binuclear structure framework in complex **3**; H atoms are omitted for clarity.

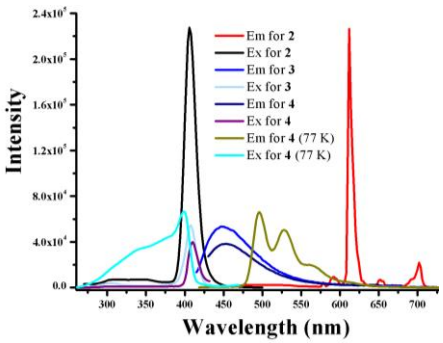

Figure 2. Emission and excitation spectra of complexes **2**-**4** in MeCN solution (10^{-5} M) at room temperature or 77 K.

system of complex **2** in PVK as the EML1 and Alq_3 as the EML2, two series of **PLEDs-I-II** were fabricated by a typical spin-coating procedure with the same configuration of ITO/PEDOT:PSS (40 nm)/PVK:complex **2** (*x*, wt% *versus* PVK) (EML1, 40 nm)/Alq_3 (EML2, 20 nm)/BCP (*y* nm)/LiF (1 nm)/Al (100 nm). For the reference **PLED-I**, *x* = 30% and *y* = 10 nm were adopted. As to **PLEDs-II** for device optimization, factors of *x* = 20% and *y* = 20 nm for **PLED-II-A**, *x* = 30% and *y* = 20 nm for **PLED-II-B** and *x* = 40% and *y* = 20 nm for **PLED-II-C** were considered, respectively.

3. Results and discussion

Synthesis, characterization and photo-physical properties of complexes [Zn(Salen)(μ-OAc)Ln(DBM)$_2$)] (Ln = La, 1; Eu, 2; Tb, 3 or Gd, 4)

The precursor [Zn(Salen)(MeCN)] was obtained with a high yield of 91% from the reaction of the typical Salen-type Schiff-base lignd H_2Salen and $Zn(OAc)_2{\cdot}2H_2O$ in dry MeCN. As shown in Scheme 1S, further reaction of the precursor with the deprotonated ligand $(DBM)^-$ and $Ln(OAc)_3{\cdot}6H_2O$ (Ln = La, Eu, Tb or Gd) in a stipulated molar ratio of 1:2:1, afforded the targeted complexes [Zn(Salen)(μ-OAc)Ln(DBM)$_2$)] (Ln = La, **1**; Ln = Eu, **2**, Ln = Tb, **3** or Ln = Gd, **4**) in the appreciable yields of 79-82%, respectively.

The compositions of the precursor [Zn(Salen)(MeCN)] and its complexes **1**-**4** were well-characterized by EA, FT-IR, ^{1}H NMR and ESI-MS. The ^{1}H NMR spectrum of the *anti*-ferromagnetic Zn^{2+}-La^{3+}-based complex **1** showed a stipulated 1:2 molar ratio of protons from $(Salen)^{2-}$ to $(DBM)^-$ in the region of 8.42-1.42 ppm. A singlet peak at 1.74 ppm indicated the presence of OAc^-. Moreover, ESI-MS spectra of complexes **1**-**4** exhibited a strong mass peak at *m/z* 1029.16 (**1**), 1043.18 (**2**), 1049.18 (**3**) or 1050.18 (**4**) assigned to the major species $[M\text{-}H]^+$ of complexes **1**-**4**, respectively. These observations show that the respective discrete hetero-binuclear [Zn(Salen)(μ-OAc)Ln(DBM)$_2$)] unit of complexes **1**-**4** is stable in the corresponding dilute solution. Molecular structure of complex **3** was also confirmed by X-ray single-crystal diffraction analysis with crystallographic data in Tables 1-2S. The complex **3** crystallizes in the monoclinic *P2(1)/n* space group. As shown in Figure 1, the Zn^{2+} ion (Zn1) located in the inner *cis*-N_2O_2 core of the $(Salen)^{2-}$ ligand is five-coordinate, and its distorted square pyramidal geometry is composed of the *cis*-N_2O_2 cavity as the base plane and one O atom (O7) of the μ-OAc^- anion at the apical position. The seven-coordinate sphere of the Tb^{3+} ion (Tb1) is saturated by two phenolic O atoms (O1 and O2) from one [Zn(Salen)] portion, four O atoms (O3-O6) from two β-diketonate $(DBM)^-$ ligands and one O atom (O8) from the μ-OAc^- anion. Two metal ions are bridged by the bidentate μ-OAc^- anion and two phenolic O atoms of the [Zn(Salen)] portion, leading to the formation of a hetero-binuclear host framework with a Zn1···Tb1 distance of 3.277(3) Å. The hetero-binuclear structure of complex **3** is almost comparable to the reported complex [Zn(Salen)Eu(tta)$_2$(μ-tfa)][24] with a similar dual-bridging feature. It is quite different from [Zn(Salen)(4-vinyl-Py)Ln(BA)$_2$(NO_3)][25] we reported early. In this structure, two metal ions were just bridged with two phenolic O atoms from one [Zn(Salen)] portion. The Zn^{2+}-Ln^{3+}-bis-β-diketonate characteristic configuration[26] is due to the involvement of one bulky [Zn(Salen)] fragment, from which, the optical absorbance is strengthened and the direct oscillator-vibrated quenching effect[27] of Ln^{3+} ion is completely prevented. More importantly, the incorporation of the light-harvesting [Zn(Salen)] portion capable of both sensitizing and electron-transporting, should have remarkable effects[24-25] on the desirable optoelectronic property for its heterometallic Zn^{2+}-Ln^{3+} complexes. Furthermore, thermogravimetric (TG) analysis (Figure 1S) of complex **2** shows its favourable thermal stability with a decomposition temperature (T_d, corresponding to 5% weight loss) up to 200 °C.

Photo-physicial properties of complexes **2**-**4** were measured in dilute MeCN solution at room temperature or 77 K, and summarized in Figures 2 and 2-3S. As shown in Figure 2S, within the similar ligands-centered absorption spectra (235-236, 259-261 and 348-349 nm) of complexes **2**-**4**, the π-π*-transited lowest energy absorption is red-shifted by 6-7 nm as compared to that of the free HDBM ligand while slightly blue-shifted relative to that of the precursor [Zn(Salen)(MeCN)] after the coordination of Zn^{2+} and/or Ln^{3+} ions. For complex **2**, the photoluminescence (Figure 2) upon λ_{ex} = 406 nm just exhibits the Eu^{3+}-centered characteristic emissions ($^5D_0 \rightarrow {}^7F_J$, *J* = 0-4), giving a bright colour-pure red-light with a CIE (Commission International de l'Éclairage) chromaticity coordinate (*x* = 0.632, *y* = 0.344). Its outstanding photoluminescence of complex **2** is further validated from the attractive quantum efficiency (Φ_{Eu}) of 40.2%, which is much greater than those[28] of Eu^{3+}-tris-β-diketonate complexes. As to complexes **3**-**4**, photo-excitation of the chromophores gives rise to the similar ligand-based fluorescence (λ_{em} = 449 nm; τ = 1.2 or 1.6 ns) assigned to the intra-ligand π-π* transition, and no Tb^{3+}-centered characteristic emissions are observed for complex **3**. In contrast, the Zn^{2+}-Gd^{3+}-complex **4** exhibits the 0-0 transition phosphorescence (λ_{em} = 496 nm and τ =

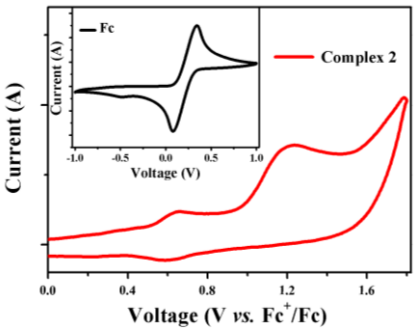

Figure 3. Cyclic voltammogram of complex **2** recorded versus Fc^+/Fc in solution at room temperature under a N_2 atmosphere (scan rate = 100 mV/s).

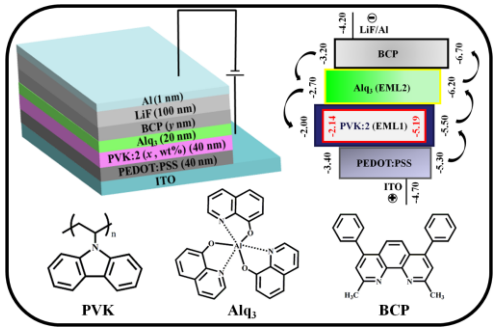

Figure 4. Double-EML-configured device structure for **PLEDs-I-II** with energy level diagram.

700 μs; also Figure 2) at 77 K, from which, the $^3\pi$-π^* triplet energy level of 20161 cm^{-1} is obtained. Therefore, the relatively lower $^3\pi$-π^* triplet energy level (20161 cm^{-1}) than the first excited state $^5D_4$ (20545 cm^{-1}) of Tb^{3+} ion should be responsible to the quenching of Tb^{3+}-centered characteristic emissions of complex **3** through non-radiative deactivation.[27] However, regulated with Latva's empirical rule,[29] the suitable energy gap ($^3\pi$-π^* - $^5D_0$; 17286 cm^{-1} of $^5D_0$ (Eu^{3+})) of 2875 cm^{-1} within the ideal 2500-4500 cm^{-1} range, confirms the effective sensitization (Figure 3S) of the Eu^{3+}-centered colour-pure red-light for complex **2**.

Structural design of PLEDs-I-II based on EML1 of PVK:complex 2 and EML2 of Alq_3

To elucidate the electronic structure of colour-pure red-light complex **2**, its electrochemical property in anhydrous CH_2Cl_2 solution was investigated and the HOMO and LUMO energy levels were calculated. In the cyclic voltammogram shown in Figure 3, a reversible oxidation process was detected at a half-wave potential of 0.39 V *versus* Fc^+/Fc for complex **2**, which could be assigned to a Eu^{3+}-centered predominant process. Due to no distinctive reduction wave for complex **2**, a reasonable E_g^{OPT} of 3.05 eV estimated from the absorption edge (406 nm; also Figure 1S) renders the calculated HOMO and LUMO energy levels of -5.19 and -2.14 eV, respectively. Both the HOMO and LUMO energy levels of complex **2** fall within those (-5.50 and -2.00 eV) of PVK with the shallow trap depths of 0.31 and 0.14 eV, respectively. This shows that PVK characteristic of excellent hole-transporting is an ideal host for phosphorescent complex **2** in the EML1 as shown in Figure 4. As to the EML2, Alq_3 possesses a high electron mobility. Its HOMO (-6.20 eV) energy level lies between those (HOMO level: -5.50 ~ -5.19 eV for the EML1; -6.70 eV for BCP) of the EML1 and the hole-blocking BCP, and the LUMO (-2.70 eV) energy level is also perfectly within those (LUMO level: -2.14 ~ -2.00 eV for the EML1; -3.20 eV for BCP) of them. This peculiar stepwise alignment of HOMO levels from the EML1 (-5.50 ~ -5.19 eV) to the EML2 (-6.20 eV) and to BCP (-6.70 eV), facilitates the transport of injected holes, whereas the stepwise LUMO levels of BCP (-3.20 eV) to the EML2 (-2.70 eV) and to the EML1 (-2.14 ~ -2.00 eV) are helpful in promoting the transport of injected electrons. As a result, charge carriers can be well confined within the wide recombination zone.[18] From the viewpoint of electro-luminescence, the following carrier-trapping and colour-compensation should occur as expected.

Electroluminescent performance of PLEDs-I-II with double-EML configuration

To realize the electroluminescent white-light, a typical dEML-configured reference device **PLED-I** was fabricated with the enactment of the complex-**2** doping concentration at 30% (wt% *versus* PVK) in the EML1, the Alq_3-adopted EML2 thickness of 20 nm and the stipulated 10 nm thickness of BCP. The electroluminescent results are summarized in Table 1 and Figure 5. As shown in Figure 5(a), the normalized electroluminescent spectra from the **PLED-I** consist of the simultaneous emissions of PVK-based blue-light (λ_{em} = 414 nm), Alq_3-centered green-light (λ_{em} = 512 nm) and Eu^{3+}-centered red-light (λ_{em} = 613 nm), which indicates that the carrier-combination area is located at the EML1/EML2 interface. Contrary to the weak enough emission of PVK-based blue-light (λ_{em} = 414

Table 1 EL properties of **PLED-I** electroluminescent properties of **PLED-I** with the doping content of 20 wt% complex **2** and BCP thickness of 10 nm and **PLEDs-II-A-C** with the doping content of complex **2** (20 wt% for **PLED-II-A**, 30 wt% for **PLED-II-B**) or 40 wt% for **PLED-II-C**) and BCP thickness of 20 nm

Device	V_{on}/V	L^{max}/cd m^{-2}	η_c^{max}/cd A^{-1}	η_p^{max}/lm W^{-1}	η_{EXE}^{max}/%	Color (CIE coordinates: *x*, *y*)
PLED-I	9.0	5.98 (12.0 V, 82.8 mA cm^{-2})	0.028 (10.0 V)	0.09 (12.0 V)	0.03 (10.5 V)	*Yellow-green* (0.410-0.415,0.503-0.508) (9.0 ~ 12.0 V)
PLED-II-A	6.0	96.83 (10.0 V, 179.7 mA cm^{-2})	0.39 (8.0 V)	0.99 (8.5 V)	0.56 (8.5 V)	White-light (0.294-0.321, 0.352-0.393) (6.0 ~ 10.0 V)
PLED-II-B	7.5	71.35 (12.0 V, 120.8 mA cm^{-2})	0.32 (10.0 V)	1.10 (10.5 V)	0.54 (10.0 V)	White-light (0.311-0.371, 0.332-0.396) (7.5 ~ 12.0 V)
PLED-II-C	7.5 V	8.16 (14.0 V, 33.7 mA cm^{-2})	0.19 (9.5 V)	0.52 (9.5 V)	0.22 (9.0 V)	*Yellow-Green* (0.387-0.468, 0.468-0.498) (7.5 ~ 14.0 V)

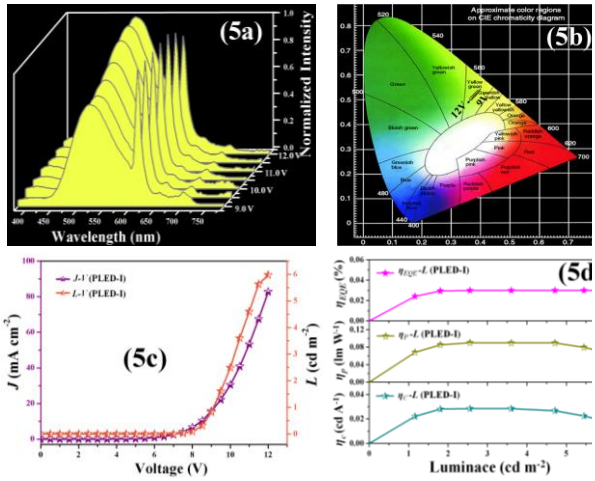

Figure 5. EL performance of **PLED-I**: (a): EL spectra; (b) CIE chromaticity coordinates; (c) *J-V-L*; (d) η_c-*L*, η_p-*L* and η_{EQE}-*L*.

nm) throughout the whole applied bias voltage range (9.0-12.0 V), the domination of the two lower energy emissions shows that effective Förster energy transfer[21] (further elucidated from the significant spectra overlap between the emission of PVK host with the absorption of complex **2** within the EML1 as shown in Figure 1S) should actually occur within the electroluminescent process. It was found that the relative intensity of the two lower energy emissions is voltage-hypersensitive. The dominated contribution of Eu^{3+}-centered red-light (λ_{em} = 613 nm) at the low applied bias voltage of 9.0, 9.5 or 10.0 V is replaced by that of Alq_3-centered green-light (λ_{em} = 512 nm) in the high applied voltage range of 10.5-12 V. We believe this arises from the emulative hole- and electron-trappings[30] within the EML1/EML2. As a result, the *tri*-chromatic colour-integrations only render the reference **PLED-I** undesirable yellow-green lights (CIE coordinates: *x* = 0.410-0.415, *y* = 0.503-0.508; Figure 5(b)). At the turn-on voltage (V_{on} at 1 cd m^{-2}; Figure 5(c)) of 9.0 V, the reference **PLED-I** is stable. With an increase of the applied bias voltage, both the luminance (*L*, cd m^{-2}) and the current density (*J*, mA cm^{-2}) monotonously increase, exhibiting a maximum luminance L^{max} of 5.98 cd m^{-2} at 12.0 V with a current density of 82.8 mA cm^{-2}. Even though the dEML-configured **PLED-I** exhibited a much lower V_{on} than those of Eu^{3+}-complex incorporated red-light PLEDs[28] or WPLEDs,[14] its inferior electroluminescent efficiencies (Table 1 and Figure 5(c); η_c^{max} = 0.028 cd A^{-1} (10.0 V); η_p^{max} = 0.09 lm W^{-1} (10.0 V) and η_{EXE}^{max} = 0.03% (10.5 V)), should result from the unbalanced carrier injection and transport within the EML1/EML2.

In consideration of the inherently higher mobility (10^{-3} cm^2 V^{-1} s^{-1}) of holes than that (10^{-6} cm^2 V^{-1} s^{-1}) of electrons during excitions' formation,[31] three dEML-configured devices **PLEDs-II-A-C** were fabricated with the increased BCP thickness (20 nm) for the strengthened hole-blocking[32] and the judicious adjustment of the doping content (20%, 30% or 40%; wt% *versus* PVK) of complex **2** in the EML1. The **PLED-II-A** with 20 wt% doping of complex **2** as shown in Table 1 and Figure 6 exhibited a strong enough blue-elementary component from excess PVK in the EML1, Eu^{3+}-centered red-light and Alq_3-based green-light. As a result, the desirable electroluminescent white-light (CIE coordinates: *x* = 0.294-0.321, *y* = 0.352-0.393; Figures 6(a) and 6(b)) in a wide range of illuminating voltages (6.0-10.0 V) was obtained. Similar to **PLED-I**, the three primary colour emissions are voltage-dependent. With an increase of the applied bias voltage, the contribution of the two higher

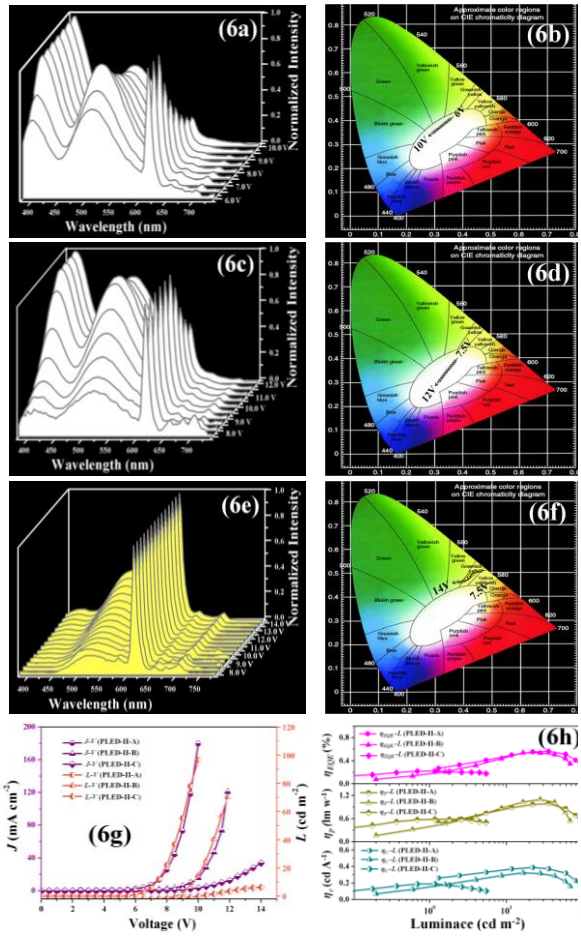

Figure 6. EL performances of **PLEDs-II-A-C**: (a): EL spectra of **PLED-II-A**; (b) CIE chromatic coordinates of **PLED-II-A**; (c): EL spectra of **PLED-II-B**; (d) CIE chromatic coordinates of **PLED-II-B**; (e): EL spectra of **PLED-II-C**; (f) CIE chromatic coordinates of **PLED-II-C**; (g) *J-V-L* of **PLEDs-II-A-C**; (d) η_c-*L*, η_p-*L* and η_{EQE}-*L* of **PLEDs-II-A-C**.

energy emissions of PVK in EML1 and Alq_3 of EML2 dominates. Convincingly, all the colour-limited white-lights for **PLED-II-A** while not yellow-green lights for **PLED-I**, should further be benefited from the increased thickness (20 nm) of BCP, enabling charge carrier balance with effective hole-blocking. As a result, the superior performance of white-light-emitting device **PLED-II-A** lies in the decreased V_{on} of 6.0 V and the significantly increased luminance (L_{max} = 96.83 cd m^{-2} at 10.0 V). Moreover, with an increase of current density or luminance, as shown in Figures 6(g) and 6(h), all the efficiencies (η_c, η_p and η_{EXE}) of **PLED-II-A** increase first, and insistently decrease with the η_c^{max} of 0.39 cd A^{-1} (8.0 V); η_p^{max} of 0.99 lm W^{-1} (8.5 V) and η_{EXE}^{max} of 0.56% (8.5 V), respectively.

Electroluminescence of devices with higher concentration of Eu^{3+}-complex was also studied. The **PLED-II-B** with 30 wt% Eu^{3+}-complex **2** in PVK gave the electroluminescent white-lights with modified CIEs coordinates (*x* = 0.311-0.371, *y* = 0.332-0.396; Figures 6(c) and 6(d)) throughout the entire voltage range (7.5-12.0 V). Under the low voltage region (7.5 ~ 9.5 V), the emission intensity of Eu^{3+}-centered red-light is relatively higher than that of Alq_3-centered green-light. In the high voltage region (10.0 ~ 12.0 V), the emission intensity of Alq_3-centered green-light increases and that of Eu^{3+}-centered red-light seems to be saturated. By comparing the *L*-

J-V characteristics of **PLED-II-B** and **PLED-II-A** shown in Figure 6(g), the relatively higher turn-on voltage of 7.5 V and the slightly decreased L_{max} of 71.35 cd m^{-2} at 12.0 V should be due to the saturation[16] of Eu^{3+}-centered red-light within the EML1/EML2. Nonetheless, because the energies tend to transfer that red dopants owing to the lower energy than the blue-light-emitting PVK host and the green-light-emitting Alq_3, **PLED-II-B** also exhibits the comparable efficiencies of η_c^{max} of 0.32 cd A^{-1} (10.0 V); η_p^{max} of 1.10 lm W^{-1} (10.5 V) and η_{EXE}^{max} of 0.54% (10.0 V) to those of **PLED-II-A**. Encouragingly, the η_{EXE}^{max} (0.54-0.56%) of the two white-light-emitting **PLEDs-II-A-B** represents a record efficiency from the previously reported organo-Eu^{3+}-based WPLEDs ($\eta_{EXE}^{max} < 0.1\%$),[14] to the best of our knowledge. Moreover, in comparison with organo-Eu^{3+} incorporated WOLEDs,[11-13] the advantages of the **PLEDs-II-A-B** lie in the good stability of white-light and the distinctively low turn-on voltages (6.0-7.5 V). Especially with the dEML-configuration with stepwise energy levels, their efficiency-roll-off is also significantly alleviated, where the η_{EXE} of 0.32% (10.0 V) for **PLED-II-A** or 0.35% (12.0 V) for **PLED-II-B** is appreciably retained, respectively. Increasing the doping content (40 wt%) of complex **2** in the EML1 for **PLED-II-C** shows that the domination of the Eu^{3+}-centered red-light makes its electroluminescent colours (CIE coordinates: x = 0.387-0.468, y = 0.468-0.498) spanning within greenish-yellow to yellow-green throughout the entire illuminating voltage range (7.5-14.0 V) as shown in Figures 6(e) and 6(f). Serious triplet-triplet annihilation and field-induced quenching effect[33] caused by the red-light-emitters' aggregation in the EML1 were observed for **PLED-II-C**, well confirming the significant decrease of photo-luminescent efficiency (Figure 4S; Φ_{em} = 15.6% for 20 wt%, 12.3% for 30 wt% or 10.4% for 40 wt%) of the reference light-emitting layer PVK:complex **2** at a high doping concentration. Consequently, with the carrier imbalance like that in **PLED-I**, the inferior electroluminescent performance (L_{max} = 8.16 cd m^{-2} (14.0 V), η_c^{max} = 0.19 cd A^{-1} (9.5 V), η_p^{max} = 0.52 lm W^{-1} (9.5 V) and η_{EXE}^{max} = 0.22% (9.0 V)) for **PLED-II-C** is also demonstrated.

4. Conclusions

In summary, colour-tunable PLEDs were realized by tuning the concentration of a Eu^{3+}-complex in the EML and the thickness of the hole-blocking BCP layer. The [Zn(salen)] in the Zn^{2+}-Eu^{3+}-bis-β-diketonate complex **2** involving decent optical absorbance and compatible triplet energy level, gives rise to the high-efficiency sensitization (Φ_{Eu} = 40.2%) of Eu^{3+}-centered colour-pure red-light. Using PVK:complex **2** as the EML1 and Alq_3 as the EML2 for the dEML device configuration under the optimized condition (20 or 30 wt% of doping content for complex **2** and 20 nm of BCP thickness), the electroluminescent efficiencies (0.32-0.39 cd A^{-1}, 0.54-0.56% and 0.99-1.10 lm W^{-1}), give the record of organo-Eu^{3+} incorporated WPLEDs. This result, together with the advantages of low turn-on voltage (6.0-7.5 V) and low efficiency-roll-off in comparison with organo-Eu^{3+} contributed WOLEDs, renders that organo-Eu^{3+} based dEML-configuration a new approach to organo-Eu^{3+} incorporated WPLEDs.

Conflicts of interest

There are no conflicts to declare.

Acknowledgements

X. Lü thanks the National Natural Science Foundation (21373160, 21173165), the Program for New Century Excellent Talents in University from the Ministry of Education of China (NCET-10-0936), the Doctoral Program (20116101110003) of Higher Education, the Science, Technology and Innovation Project (2012KTCQ01-37) of Shaanxi Province, the MOE Laboratory of Bioinorganic and Synthetic Chemistry, the Graduate Innovation and Creativity Fund (YZZ17127) and Wisteria Scientific Research Cooperation Special Project of Northwest University in P. R. of China for the support of this work. H. He thanks the National Science Foundation (1507871) in United States for the support of this work. W.-Y. Wong thanks the Hong Kong Polytechnic University (1-ZE1C and 847S) for the financial support.

Notes and references

1 (a) M. M. Shang, C. X. Li and J. Lin, *Chem. Soc. Rev.*, 2014, **43**, 1372-1386; (b) M. Pan, W. M. Liao, S. Y. Yin, S. S. Sun and C. Y. Su, *Chem. Rev.*, 2018, **118**, 889-8935.

2 (a) S. V. Eliseeva and J.-C. G. Bünzli, *Chem. Soc. Rev.*, 2010, **39**, 189-227; (b) A. Birkel, K. A. Denault, N. C. George and R. Seshadri, *Mater. Matters*, 2012, **7**, 22-27.

3 (a) H. A. Hoeppe, *Angew. Chem. Int. Ed.*, 2009, **48**, 3572-3582; (b) A. M. Kaczmarek and R. V. Deun, *Chem. Soc. Rev.*, 2013, **42**, 8835-8848; (c) Y.-C. Lin, M. Karlsson and M. Bettinelli, *Top. Curr. Chem.*, 2016, **374**, 1-47.

4 S. Seethaleksmi, A. R. Ramya, M. L. P. Reddy and S. Varughese, *J. Photochem. Photobio. C: Photochem. Rev.*, 2017, **33**, 109-131.

5 (a) H. Iwanaga, A. Amano, H. Aiga, K. Harada and M. Oguchi, *J. Alloys Comp.*, 2006, **408-412**, 921-925; (b) G. Shao, Y. Li, K. J. Feng, F. Gan and M. L. Gong, *Sen. Actuators, B: Chem.*, 2012, **173**, 692-697; (b) R. Boddula, K. Singh, S. Giri and S. Vaidyanathan, *Inorg. Chem.*, 2017, **56**, 10127-10130; (b) K. Singh, R. Boddula and S. Vaidyanathan, *Inorg. Chem.*, 2017, **56**, 9376-9390.

6 (a) Y. Lu and B. Yan, *Chem. Commun.*, 2014, **50**, 15443-15446; Y. W. Zhao, F. Q. Zhang and X. M. Zhang, *ACS Appl. Mater. & Interfaces*, 2016, **8**, 24123-24130; (b) T. Song, G. G. Zhang, Y. J. Cui, Y. Yang and G. D. Qian, *CrystEngComm*, 2016, **18**, 8366-8371.

7 (a) J. H. Zhang, S. M. Gong, J. B. Yu, P. Li, X. J. Zhang, Y. W. He, J. B. Zhou, R. Shi, H. R. Li, A. Y. Peng and J. Wang, *ACS Appl. Mater. Interfaces*, 2017, **9**, 7272-7281; (b) C. Y. Sun, X. L. Wang, X. Zhang, C. Qin, P. Li, Z. M. Su, D. X. Zhu, G. G. Shan, K. Z. Shao, H. Wu and J. Li, *Nat. Comm.*, 2013, **4**, 3717; (c) D. Q. Yang, Y. Xu, Y. L. Yao, J. H. Zhang, J. Wang and Y. G. Wang, *Synth. Met.*, 2016, **221**, 236-241.

8 (a) X. G. Huang, G. Zucchi, J. Tran, R. B. Pansu, A. Brosseau, B. Geffroy and F. Nief, *New. J. Chem.*, 2014, **38**, 5793-5800; (b) T. V. Usha Gangan and M. L. P. Reddy, *Dalton Trans.*, 2015, **44**, 15924-15937;

9 N. Thejo Kalyani and S. J. Dhoble, *Renew. Sust. Energy Rev.*, 2012, **16**, 2696-2723.

10 J. Kido, W. Ikeda, M. Kimura and K. Nagai, *Jpn. J. Appl. Phys.*, 1996, **35**, L394-L396.

11 G.-L. Law, K.-L. Wong, H.-L. Tam, K.-K. Cheah and W.-T. Wong, *Inorg. Chem.*, 2009, **48**, 10492-10494.

12 (a) D. X. Zhao, W. L. Li, Z. R. Hong, X. Y. Liu, C. J. Liang and D. Zhao, *J. Lum.*, 1999, **82**, 105-109; (b) S. W. Pyo, S. P. Lee, H. S. Lee, O. K. Kwon, H. S. Hoe, Y.-K. Ha, Y. K. Kim and J. S. Kim, *Thin*

Solid Films, 2000, **363**, 232-235; (c) S. F. Li, G. Y. Zhong, W. H. Zhu, F. Y. Li, J. F. Pan, W. Huang and H. Tian, *J. Mater. Chem.*, 2005, **15**, 3221-3228; (d) W. G. Quirino, C. Legnani, M. Cremona, P. P. Lima, S. A. Junior and O. L. Malta, *Thin Solid Films*, 2006, **494**, 19-47; (e) G. Zucchi, T. Jeon, D. Tondelier, D. Aldakov, P. Thuéry, M. Ephritikhine and B. Geffroy, *J. Mater. Chem.*, 2010, **20**, 2114-2120; (f) L. L. Chen, B. B. Wang, L. M. Zhang, D. X. Zhu, P. Li, Z. M. Su and B. Li, *Solid-State Electron.*, 2012, **69**, 67-71; (g) P. P. Lima, F. A. A. Paz, C. D. S. Brites, W. G. Quirion, C. Legnani, M. C. e Silva, R. A. S. Ferreira, S. A. Junior, O. L. Malta, M. Cremona and L. D. Carlos, *Org. Electron.*, 2014, **15**, 798-808.

13 S. Biju, L. J. Xu, C. Z. Sun and Z. N. Chen, *J. Mater. Chem. C*, 2015, **3**, 5775-5782.

14 (a) Y. Hino, H. Kajii and Y. Ohmori, *Jpn. J. Appl. Phys.*, 2007, **46**, 2673-2677; (b) U. Giovanella, M. Pasini, C. Freund, C. Botta, W. Porzio and S. Destri, *J. Phys. Chem. C*, 2009, **113**, 2290-2295; (c) J. Mezyk, W. Mróz, A. Mech, U. Giovanella, F. Meinardi, C. Botta, B. Vercelli and R. Tubino, *Phys. Chem. Chem. Phys.*, 2009, **11**, 10152-10156; (d) R. Grykien, B. Luszczynska, I. Glowacki, L. Puntus, I. Pekareva, K. Lyssenko, F. Kajzar, I. Rau and C. A. Lazar, *Opt. Mater.*, 2016, **57**, 114-119; (e) B. N. Li, L. Liu, G. R. Fu, Z. Zhang, H. Y. Li, X. Q. Lü, W.-K. Wong and R. A. Jones, *J. Lumin.*, 2017, **192**, 1089-1095.

15 J. Kido and Y. Okamot, *Chem. Rev.*, 2002, **102**, 2357-2368.

16 C. Adachi, M. A. Baldo and S. R. Forrest, *J. Appl. Phys.*, 2000, **87**, 8049-8055.

17 (a) X. Zhou, D. S. Qin, M. Pfeiffer, J. Blochwitz-Nimoth, A. Werner, J. Drechsel, B. Maennig, K. Leo, M. Bold, P. Erk and H. Hartmann, *Appl. Phys. Lett.*, 2002, **81**, 4070-4072; (b) G. He, M. Pfeiffer, K. Leo, M. Hofmann, J. Birnstock, R. Pudzich and J. Salbeck, *Appl. Phys. Lett.*, 2004, **85**, 3911-3913.

18 (a) L. Zhou, C.-C. Kwok, G. Cheng, H. J. Zhang and C.-M. Che, *Opt. Lett.*, 2013, **38**, 2373-2375; (b) L. Zhou, C.-L. Kwong, C.-C. Kwok, G. Cheng, H. J. Zhang and C.-M. Che, *Chem. Asian J.*, 2014, **9**, 2984-2994; (c) L. Zhou, L. J. Li, Y. L. Jiang, R. Z. Cui, Y. N. Li, X. S. Zhao and H. J. Zhang, *ACS Appl. Mater. Interfaces*, 2015, **7**, 16046-16053.

19 F. Z. Shen, H. Xia, C. B. Zhang, D. Lin, L. He and Y. G. Ma, *J. Phys. Chem. B*, 2004, **108**, 1014-1019.

20 H.-P. Lin, F. Zhou, J. Li, X.-W. Zhao, L. Zhang, X.-L. Jiang, Z.-L. Zhang and J.-H. Zhang, *J. Phys. Chem. C*, 2011, **115**, 24341-24346.

21 (a) Z. J. Wang and I. D. W. Samuel, *J. Lumin.*, 2005, **111**, 199-203; (b) S. Moynihan, D. Iaconpino, D. O' Carroll, H. Doyle, D. A. Tanner and G. Redmond, *Adv. Mater.*, 2007, **19**, 2474-2479; (c) L. Liu, M. Y. Pang, H. T. Chen, G. R. Fu, B. N. Li, X. Q. Lü and L. Wang, *J. Mater. Chem. C*, 2017, **5**, 9021-9027; (d) G. R. Fu, J. Q. Guan, B. N. Li, L. Liu, Y. N. He, C. Yu, Z. Zhang and X. Q. Lü, *J. Mater. Chem. C*, 2018, **6**, 4114-4121.

22 S. L. Gong, C. L. Yang and J. G. Qin, *Chem. Soc. Rev.*, 2012, **41**, 4797-4807.

23 C. Yu, Z. Zhang, L. Liu, H. Y. Li, Y. N. He, X. Q. Lü, W.-K. Wong and R. A. Jones, *New J. Chem.*, 2015, **39**, 3698-3707.

24 S. M. Wang, B. Zhang, Y. H. Hou, C. X. Du and Y. J. Wu, *J. Mater. Chem. C*, 2013, **1**, 406-409.

25 L. Liu, X. Y. Zhang, G. R. Fu, X. Q. Lü, W.-K. Wong and R. A. Jones, *Dyes Pigm.*, 2017, **141**, 137-147.

26 P. A. Vigato, V. Peruzzo and S. Tamburni, *Coord. Chem. Rev.*, 2009, **253**, 1099-1201.

27 (a) L. J. Xu, G. T. Xu and Z. N. Chen, *Coord. Chem. Rev.*, 2014, **273-274**, 47-62; (b) J.-C. G. Bünzli, *Coord. Chem. Rev.*, 2015, **293-294**, 19-47.

28 H. Xu, Q. Sun, Z. F. An, Y. Wei and X.-G. Liu, *Coord. Chem. Rev.*, 2015, **293-294**, 228-249.

29 M. Latva, H. Mukkala, C. Matachescu, J. C. Rodriguez-Ubis and J. Kanakare, *J. Lumin.*, 1997, **175**, 149-169.

30 (a) L. Yin, C.-L. Ho, H. B. Wu, Y. Cao and W.-Y. Wong, *Adv. Mater.*, 2014, **26**, 2459-2473; (b) X. L. Yang, G. J. Zhou and W.-Y. Wong, *J. Mater. Chem.C*, 2014, **2**, 1760-1778.

31 Y. Shirota and H. Kageyama, *Chem. Rev.*, 2007, **107**, 953-1010.

32 A. P. Pereira, H. Gallardo, G. Conte, W. G. Quirino, C. Legnani, M. Cremona and I. H. Bechtold, *Org. Electron.*, 2012, **13**, 90-97.

33 W. S. Jeon, T. J. Park, S. Y. Kim, R. Pode, J. Jang and J. H. Kwon, *Appl. Phys. Lett.*, 2008, **93**, 063303.

Table of content

Efficient white polymer light-emitting diodes (WPLEDs) based on double emitting layers of PVK:Eu(III)-complex and Alq_3

Yani He, Lin Liu, Guorui Fu, Wentao Li, Xingqiang Lü, Hongshan He and Wai-Yeung Wong

Elaborated from the dEML-configured structure and the optimized condition (Eu^{3+}-complex-doping and hole-blocking) for WPLEDs with low turn-on voltage (6.0-7.5 V) and low efficiency-roll-off, their efficiencies (η_c = 0.32-0.39 cd A^{-1}, η_{EQE} = 0.54-0.56% and η_p = 0.99-1.10 lm W^{-1}), represent the record of organo-Eu^{3+} incorporated WPLEDs.